Desalination and Water Treatment
www.deswater.com

doi: 10.5004/dwt.2023.29863

307 (2023) 18–29
September

MOF and GO containing interpenetrated polymers for high throughput desalination

Masoud Jafarian, Akbar Malekpour*, Gholam Ali Koohmareh

Department of Chemistry, University of Isfahan, Isfahan, 81746/73441, Iran, emails: a.malekpour@chem.ui.ac.ir (A. Malekpour), Jafarian_masoud@yahoo.com (M. Jafarian), Tel.: +98 3137934931; email: G.a.koohmareh@chem.ui.ac.ir (G.A. Koohmareh)

Received 14 April 2023; Accepted 6 August 2023

ABSTRACT

Composite membranes consisting of PVA/PAA as interpenetrating polymer networks (IPN), along with various MOFs (MIL-101-Cr, Cu-BTC, UiO-66-NH_2) or graphene oxide (GO), were synthesized using a sequential method. These membranes were designed for use in the pervaporation desalination of NaCl and $MgCl_2$ salts. The membranes were characterized using swelling, contact angle, FTIR, tensile, and SEM tests, and the optimal preparation parameters were determined using an experiment design method. Subsequently, the optimal membranes were employed in the pervaporation desalination process, with salt rejection and fluxes serving as the pervaporation responses. The results showed that as the temperature of the feed increased, the water flux also increased. However, as the feed solution temperature and concentration increased, the salt rejection decreased. Under optimal conditions, the IPN/MIL-101-Cr membrane provided 15.19 and 14.59 kg/m^2·h flux and 99.24% and 99.37% rejection for sodium and magnesium ions, respectively, while the GO/IPN membrane provided 13.65 and 12.98 kg/m^2·h flux and 98.97% and 99.10% rejection for sodium and magnesium ions, respectively. These composite membranes also exhibited excellent performance in salt mixtures. Based on the experimental design results, preliminary evaluation tests, and comparison with other membranes, it can be concluded that the IPN/MIL-101-Cr composite membrane is highly effective for pervaporation desalination and has potential for industrial-scale applications.

Keywords: Composite IPN membrane; MOF; MIL-101-Cr; Graphene oxide; Desalination; Pervaporation; Cu-BTC; UiO-66-NH_2; Interpenetrating polymer network

1. Introduction

Water scarcity has become a global concern in recent decades, and as a result, the desalination of seawater has been introduced as a solution to this problem. Seawater accounts for about 97.5% of the world's water, making it a plentiful source for desalination and water supply [1]. There are several desalination methods in use, including reverse osmosis [2], multistage distillation [3], and electro dialysis [4]. However, some of these methods have limitations that have yet to be addressed. For example, reverse osmosis has a high energy consumption that can be reduced with the use of energy recovery devices or pretreatment processes [5]. Heat distillation methods consume a significant amount of energy [6]. Additionally, some membrane methods can be affected by free chlorine ion [7] or crystalline accumulation on the membrane surface, leading to membrane closure [8]. Pervaporation is an alternative membrane-based separation process that operates on the basis of differences in solubility or penetration into the membrane, unlike conventional distillation methods that rely on vapor-liquid equilibrium.

One advantage of pervaporation is its ability to perform well with azeotrope solutions. To ensure proper separation, the membrane must interact effectively with the separating components [9]. For instance, to dehydrate a

* Corresponding author.

solution, hydrophilic polymers such as polyvinyl alcohol [10] or polyacrylic acid, which contain hydroxyl and carboxyl hydrophilic groups respectively, are used. However, one major disadvantage of hydrophilic membranes is that they tend to swell in the presence of water. This not only allows water to pass through the membrane but also other particles in the solution, reducing the membrane's selectivity [11]. To address this issue, various methods have been developed, including the use of cross-linkers [12], combining the membrane with low-swelling polymers [13], forming copolymers with hydrophobic polymers [14], or using composite membranes [15] that prevent swelling. Pervaporation also finds application in desalination.

In pervaporation, a significant portion of the solution passes through the membrane and permeates as a vapor. The advantages of using pervaporation for desalination include high salt rejection, particularly for monovalent salts [16–18], prevention of organic material passage through hydrophilic membranes, and low occurrence of issues such as membrane wetting, salt deposition, and pore blocking. As pervaporation is a phase evaporation process that does not involve osmotic pressure, it can be used to desalinate solutions with very high salt concentrations, without the need to correct for vapor pressure differences across the membrane [19]. Due to these benefits, research on pervaporation for desalination has increased significantly. Pervaporation has been employed for desalination using a range of polymer membranes. For instance, Liang et al. [20] used a sulfonated polyethylene membrane, Sule et al. [21] used a polyester membrane, Naim et al. [22] used a cellulose acetate membrane, Wang et al. [23] used a poly(styrene-ethylene/butylene-styrene) block copolymer membrane, da Silva et al. [24] used a silica/PVA membrane, and Zhao et al. [25] used a poly(acrylic acid)-Fe_3O_4 composite membrane. The samples were desalinated by the pervaporation method.

Interpenetrating polymer network (IPN) membranes can reduce the high swelling rate of polymer membranes that leads to decreased performance [26]. These membranes consist of two interlocking polymer networks held together by a cross-linker, resulting in increased resistance to swelling [27]. However, the presence of two cross-linking networks can reduce the amount of water passing through the membrane. To address this issue, the amount of transition phase can be increased by adding materials and fillers. One approach is to use composite IPN membranes that incorporate materials such as MOFs [28], zeolites [29–31], or graphene oxide [32]. By incorporating fillers into the polymer matrix, the properties of the membrane can be tailored to achieve improved selectivity, permeability, and mechanical strength.

In a previous study [33], desalination was performed using reverse osmosis and pervaporation with cross-linked polymer, IPN, and IPN/zeolite composite membranes, and their performance was compared. The composite membrane demonstrated superior performance to the other two membranes.

MO-F-Alg(Cu)/PVA membrane was utilized by Bhattacharjee et al. [34] for desalination of seawater. Meanwhile, Zhao et al. [35] employed a polyvinylpyrrolidone-UiO-66-NH_2 membrane to eliminate dyes. For desalination of saline water, Xu et al. [36] used a ZIF-8/tannic acid-polyethersulfone membrane. Rajput et al. [37] removed salts using an IPN (polyvinylchloride/styrene/divinylbenzene)/sulfonated graphene oxide composite membrane. Finally, Ghazi and Bagherian [38] separated methylene blue dye by using MIL-101(Cr) dispersed in a thin-film polyvinyl alcohol membrane.

In this study, composite IPN membranes with MOF fillers such as MIL-101-Cr [39], Cu-BTC [40], UiO-66-NH_2 [41], and GO [42] were used for the desalination of aqueous solutions via pervaporation. These fillers have characteristics such as hydrophilicity, high stability, large surface area, availability and simplicity in synthesis. Several MOFs were investigated and compared with plain IPN membranes. A design of experiments approach was used to optimize membrane preparation and performance.

2. Experimental setup

2.1. Materials

Polyvinyl alcohol (PVA) with a molecular weight of 125,000 was synthesized from Merck Co. Acrylic acid (AA) was used as a guest monomer, and ethylene glycol dimethacrylate (EGDMA) was used as a cross-linker, while benzoyl peroxide (BPO) was used as an initiator of polymerization, all of which were provided by Merck Co. Glutaraldehyde (GA) and HCl (37%) were used as a cross-linker and catalyst, respectively. NaCl and $MgCl_2$ were obtained from Merck Co., and NaOH was used to neutralize the acidic property. Chromium terephthalate metal-organic framework (MIL-101-Cr) [43], Copper 1,3,5-benzenetricarboxylate metal–organic framework (Cu-BTC) [44], Zr-based metal–organic frameworks functionalized with an amine group (UiO-66-NH_2) [41], and graphene oxide (GO) [42] were used as fillers for the membranes and were prepared as described in the previous literature.

The method used to prepare the composite membranes is similar to the one used for the composite IPN/Zeolite membrane in our previous study [33]. To prepare the composite IPN membrane, the filler was added to water at 70°C and completely dispersed. Next, PVA was mixed for two or three hours in DI water at 70°C. Then, AA, BPO, and EGDMA were added to this solution as the guest monomer, polymerization initiator, and PAA cross-linker, respectively. The mixture was then stirred at 70°C for 12 h. Once the temperature reached ambient levels, 0.2 mL of GA was added as a cross-linker, and 0.5 g of HCl was added as a catalyst, and the mixture was stirred for 20 min. The resulting solution was poured into a molding container before it stiffened completely and was kept at ambient temperature for 24 h. To ensure cross-linking, the membrane was placed in an oven at 100°C for 5 h. The membrane was then washed with NaOH solution to remove excess HCl and then washed several times with water to remove excess salt. Finally, the membrane was dried at room temperature.

2.2. Characterization of membranes

To determine the swelling of each membrane, the following formula was used:

$$\text{Swelling percentage } \% = \left(\frac{\left(W_W - W_d\right)}{W_d} \right) \times 100 \quad (1)$$

where W_w is the weight of the swollen membrane in water for 48 h, and W_d is the weight of the dried membrane. The contact angle method was used to investigate the hydrophilicity of the membranes. A more hydrophilic membrane results in an increased amount of spreading water drop and a reduced contact angle between water and the membrane. The structural characterization of the membranes was carried out using ATR-FTIR with a Jasco-6300 instrument. Tensile testing was performed on two membranes using a Santam-20 machine with a rectangular section and a 20 mm gage length at room temperature and a 5 mm/min extension speed. The mechanical resistance was determined based on the ingredients. To study the membrane morphology, the membranes were examined using a Quanta FEG-450 SEM under high vacuum conditions at 10 kV.

2.3. Setup

For pervaporation, a module was set up consisting of two separated parts that were clamped together using clamps. One part of the module was connected to a vacuum pump, with the outlet connected to a trap kept at low temperature using liquid nitrogen. The other part of the module was connected to a rotary pump linked to the feed solution. The vacuum of the vacuum pump was approximately 20 kPa. The feed tank was attached to a heater and thermostat that could be used for temperature programming. The length of each experiment was 15 min.

2.4. Pervaporation responses

Flux (J) is the amount of water passing through the membrane and can be calculated using the following formula:

$$J = \frac{Q}{A \cdot t\left(\text{kg/m}^2.\text{h}\right)} \quad (2)$$

where Q is the amount of passing solution, A is the area of the membrane, and t is the time of the experiment in h.

Rejection refers to the amount of salt rejected by the membrane. The concentration of Na^+ and Mg^{2+} ions, chosen to represent the membrane rejection efficiency, was measured using an atomic spectrophotometer (Shimadzu AA-670). Standard samples of each ion were analyzed in the instrument, and the amount of salt in the solution passing through the membrane was obtained based on the calibration curve.

3. Results and discussion

3.1. Selection of the best effective composite IPN membrane

The pervaporation method was used to conduct in vitro flux testing on four fillers, namely UiO-66-NH_2, Cu-BTC, MIL-101-Cr MOFs, and GO, as shown in Fig. 1. Each composite IPN membrane was pervaporated five times at room temperature with each filler, and it was discovered that the membrane containing MIL-101-Cr filler produced the highest flux, followed by graphene oxide and then Cu-BTC. Based on these findings, the two best-performing composite membranes (MIL-101-Cr and GO) were selected for membrane preparation and method optimization. Factors such as increased hydrophilicity, the presence of more absorbent spaces with suitable sizes for water absorption, and improved stability under operating conditions, were identified as potential contributors to increased water flux through the membranes.

3.2. Swelling test

To evaluate the swelling of the two selected composite membranes, the dry membranes were weighed and then immersed in water for 24 h. Excess water was then removed, and the weighing operation was repeated (Fig. 2). The results showed that the membrane with MIL-101-Cr was more swollen than the GO membrane. In order to assess the level of swelling in the two composite membranes under investigation, the dry membranes were initially weighed and then submerged in water for a period of 24 h. After excess water was removed, the membranes were weighed again (as depicted in Fig. 2). The results revealed that the membrane containing MIL-101-Cr exhibited a greater degree of swelling than the GO membrane. This can be attributed to the hydrophilic nature of the MIL-101-Cr filler, which is likely due to its high specific surface area and numerous unsaturated metal sites.

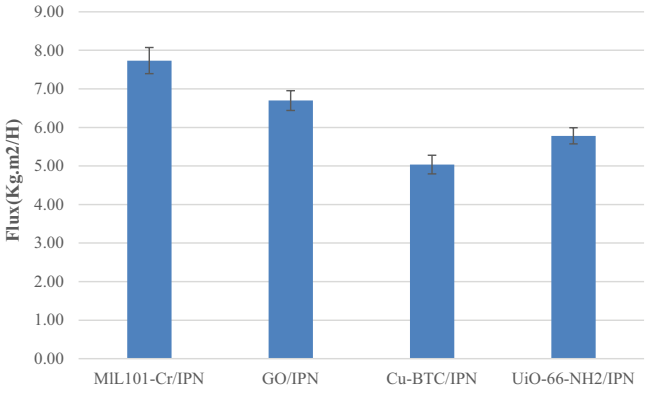

Fig. 1. Flux of composite/IPN membranes.

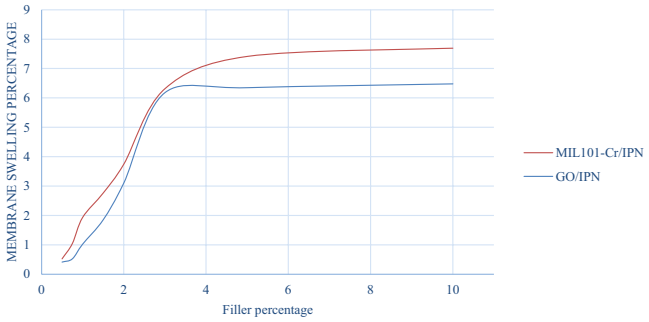

Fig. 2. Swelling test of MIL-101-Cr/IPN and GO/IPN.

3.3. Contact angle test

Based on the images obtained (as shown in Fig. 3), the contact angle between the water droplet and the MIL-101-Cr membrane was found to be significantly lower (61°) than that of the GO membrane (81.4°). A lower contact angle indicates a more hydrophilic membrane surface, as the water droplet is more readily absorbed by the membrane. This can be attributed to the higher hydrophilicity of the MIL-101-Cr membrane, which is likely due to its inherent properties.

3.4. FTIR test

The FTIR spectra of the membranes is shown in Fig. 4. The MIL-101-Cr spectrum shows a characteristic peak at 3,814 related to the Cr–OH bond [45]. Peaks at 1,640 and 1,410 correspond to the symmetric and asymmetric vibrations of COO, respectively, confirming the presence of a dicarboxylate linker in the substance [46]. These findings confirm the presence of MOF in the membrane.

In the IR spectrum of the graphene oxide/IPN membrane, peaks at 1,372 and 1,289 correspond to C–OH and C–O–C stretching vibrations, respectively, while peaks at 1,718 and 1,620 correspond to C=O and C=C bond vibrations, respectively [47]. In both spectra, the broad peak in the region between 3,500 and 3,000 is related to the O–H intermolecular hydrogen bond between IPN and the functional group of the fillers [48]. Based on the peaks observed in the IR spectrum of the two membranes, it is possible to confirm the proper synthesis of the membranes and the presence of filler in the substrate of the IPN membrane.

3.5. Tensile test

Based on the data obtained (as illustrated in Fig. 5), the MIL-101-Cr membrane exhibited greater tensile strength, withstanding a higher amount of force before breaking (42 N). Generally, the incorporation of fillers into a polymer network can disrupt the order of the network, thereby reducing the membrane's resistance. Furthermore, uneven dispersion of particles within the membrane can create asymmetric areas of resistance, leading to membrane failure in those regions. However, the presence of strong bonds between the interpenetrating polymer network (IPN) and MIL-101-Cr likely contributes to the increased strength of the MIL-101-Cr membrane. In contrast, the GO membrane showed greater elongation at its maximum tolerable force (1.9 mm) and exhibited behavior more similar to that of the IPN membrane. This may be because GO disrupts the IPN network to a lesser extent, thus maintaining a more ordered structure.

3.6. Scanning electron microscopy

As shown in the images (Fig. 6), the filler particles are well dispersed in the membrane tissue, and their dimensions are almost equal. Additionally, there is not much empty space between the particles, indicating proper dispersion of the particles during membrane preparation. Based on the images, the MIL-101-Cr and GO particle sizes are estimated to be about 300–500 and 100–200 nm, respectively.

3.7. Optimization of composite membranes

To optimize the preparation of composite membranes, the CCD experimental design method (central cube design)

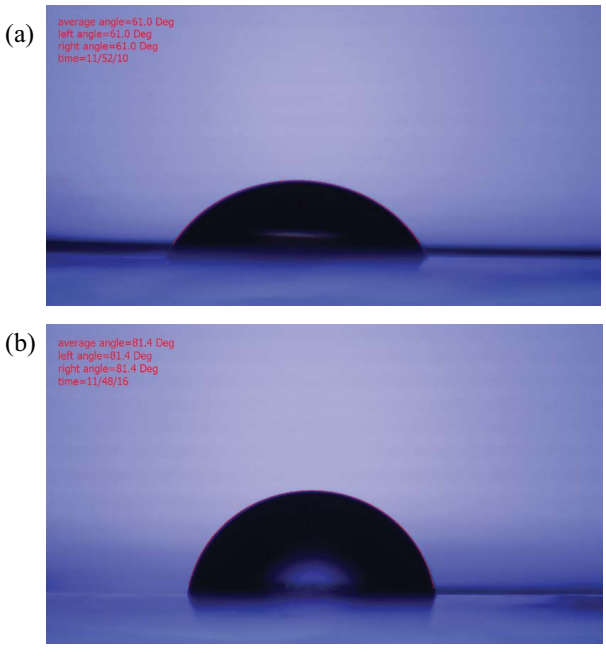

Fig. 3. Contact angel test, (a) MIL-101-Cr/IPN and (b) GO/IPN.

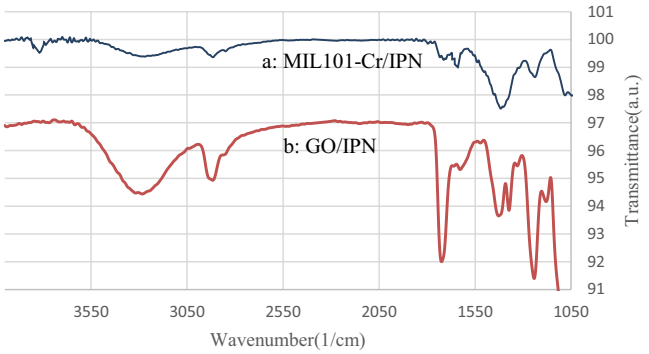

Fig. 4. FTIR test, (a) MIL-101-Cr/IPN and (b) GO/IPN.

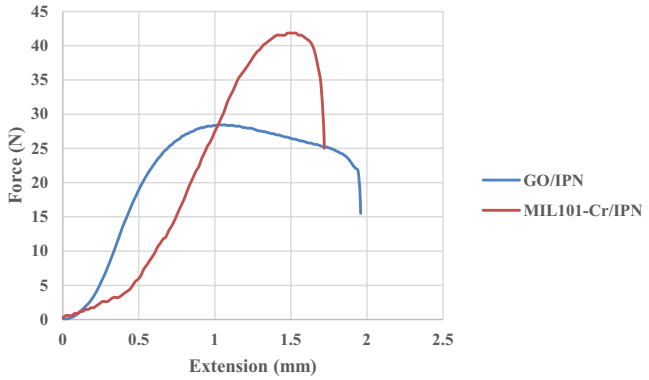

Fig. 5. Tensile test of MIL-101-Cr/IPN and GO/IPN.

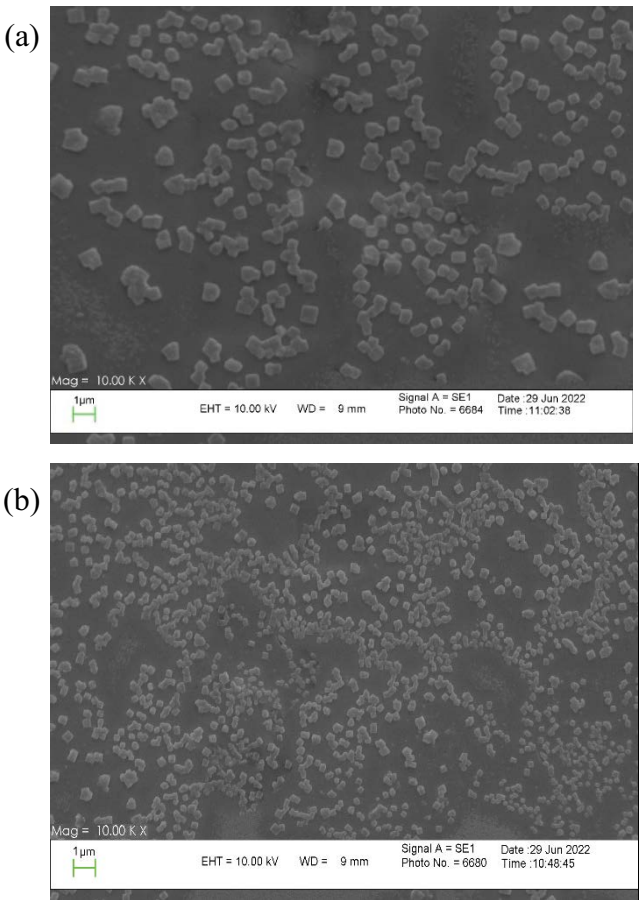

Fig. 6. SEM, (a) MIL-101-Cr/IPN and (b) GO/IPN.

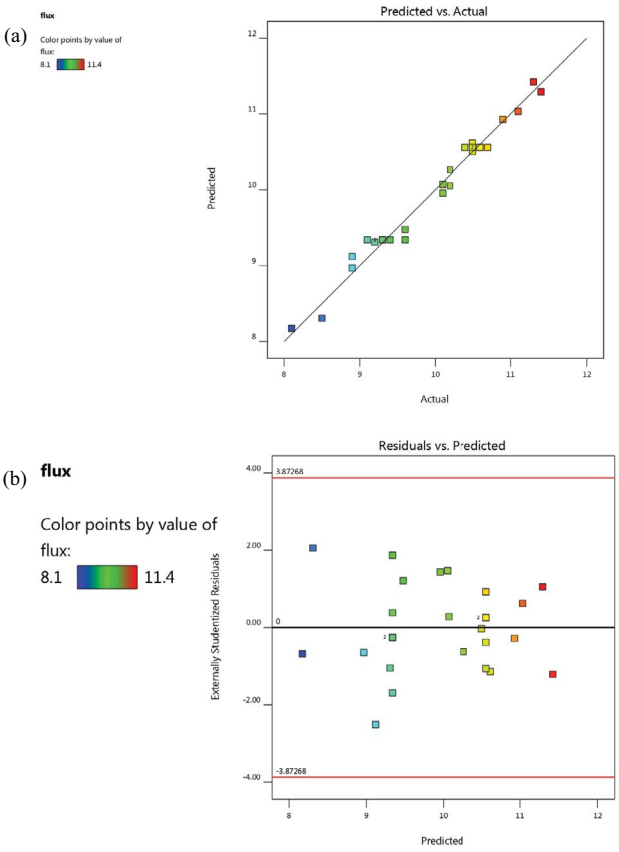

Fig. 7. Actual and residuals vs. predicted diagram.

was used. The parameters in the membrane preparation were the amount of filler and the amount of IPN cross-linker. The response in this method was the flux passing through the membrane. After performing the experimental design and ANOVA review, it was found that the obtained model did not have a significant lack of fit and was quite significant. The actual and predicted data were completely consistent with each other (Fig. 7). Based on the equation, it was found that the amount of filler, the amount of cross-linker, as well as the time of adding the filler to the solution, were influential parameters in this design.

The predicted R^2 of 0.9057 was in reasonable agreement with the adjusted R^2 of 0.9630, with the difference being less than 0.2. Adequate precision measures the signal-to-noise ratio, and a ratio higher than 4 is desirable. The ratio in the experimental design was 28.3, showing that the signals were completely adequate. This model can be used to navigate the design space. The coefficient of variation (CV) of the method was 1.67%, indicating that the method was accurate.

According to the obtained data, as the amount of filler increased, the amount of flux also increased (Fig. 8). This increase may be due to the increase in the amount of water passing areas on the membrane surface. As the amount of cross-linker increased, the amount of flux decreased. This may be because, with an increase in cross-linker, the amount of pores in the membrane decreased, and the membrane became more rigid.

The composite membrane with MIL-101-Cr created more flux (11.4 kg/m^2·h) than graphene oxide (10.3 kg/m^2·h), which may be due to the MIL-101-Cr filler being more hydrophilic. Therefore, based on the obtained results, optimum values were used to prepare the membrane for use in pervaporation.

3.8. Optimization of pervaporation

To optimize pervaporation using two composite membranes, GO and MIL-101-Cr, the CCD method was used. Two feed solutions containing sodium ion (NaCl) and magnesium ion ($MgCl_2$) were used. Factors affecting pervaporation were feed temperature, feed pH, feed concentration, membrane type, and ion type. The responses were the flux across the membrane and the amount of salt rejection. After reviewing the CCD and ANOVA results, it was found that the model was quite significant in both flux and rejection. The actual and predicted data were completely consistent with each other (Fig. 9).

For flux, feed temperature (T), feed concentration (C), feed pH, membrane type, ion type, interaction between T-C, T-membrane type, T-T, and C-C were effective factors in this experimental design. For salt rejection, T, C, feed pH, membrane type, ion type, interaction between T-C, C-membrane type, T-T, and C-C were effective factors (Table 1).

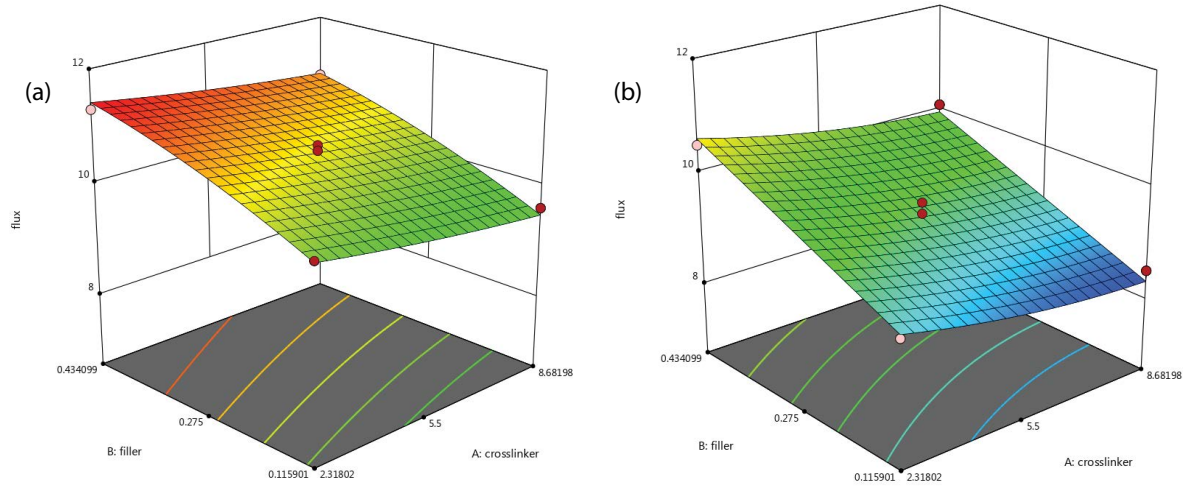

Fig. 8. 3D chart, (a) flux vs. filler vs. cross linker for MIL-101-Cr/IPN and (b) flux vs. filler vs. cross linker for GO/IPN.

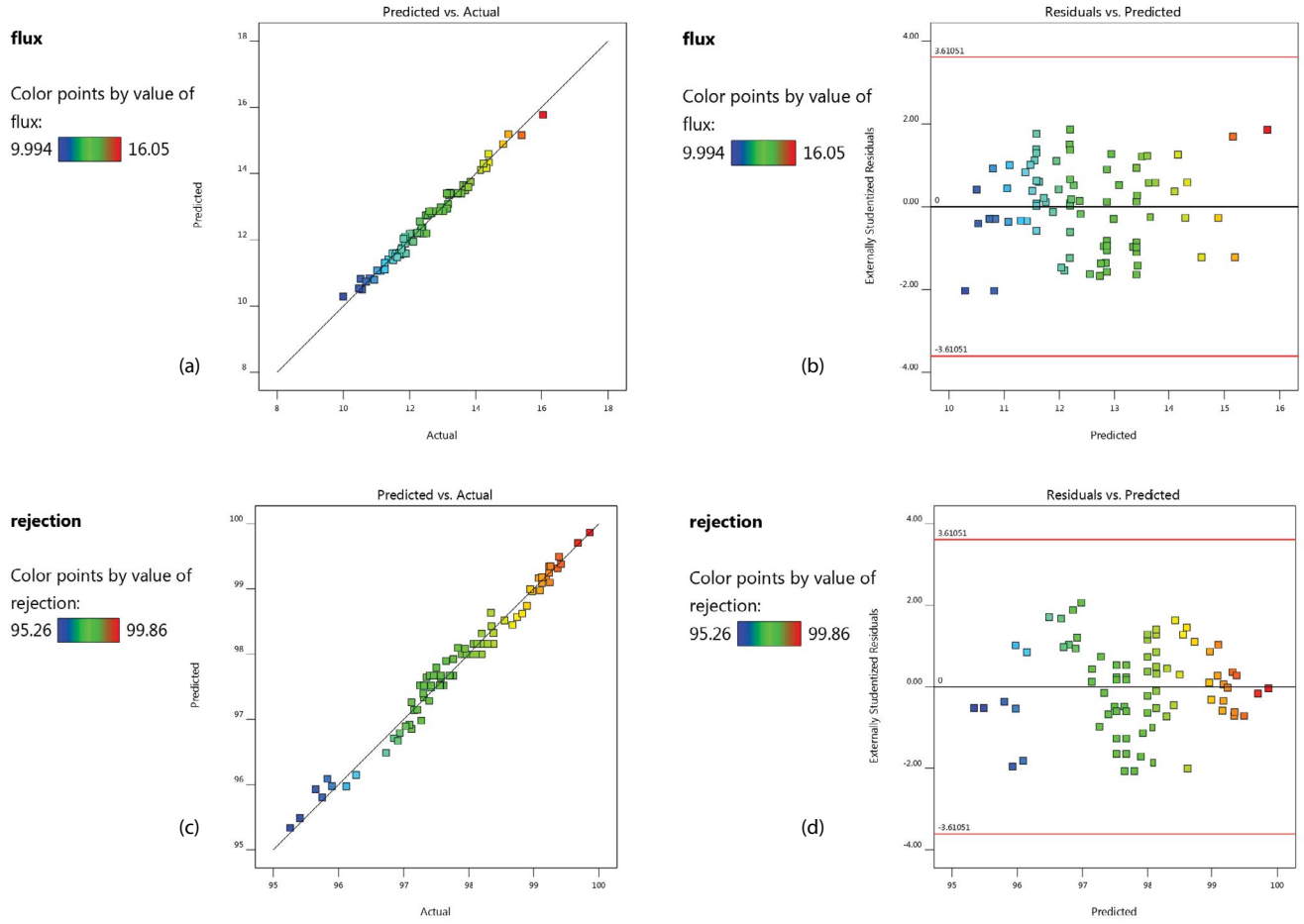

Fig. 9. Actual and residuals vs. predicted diagram, (a) flux and (b) salt rejection.

For flux, the predicted R^2 of 0.9695 was in reasonable agreement with the adjusted R^2 of 0.9773, with adequate precision of 62.77 and CV of 1.43%. For salt rejection, the predicted R^2 of 0.9609 was in reasonable agreement with the adjusted R^2 of 0.9721, with adequate precision of 53.48 and CV of 0.17%. All the data showed the appropriateness of the proposed model in the CCD.

According to the obtained three-dimensional charts, the amount of flux in both membranes and both ions increased with an increase in temperature (Fig. 10). This increase

Table 1
Final equations of model

Ion: Na Membrane: MIL-101-Cr/IPN	Flux equation	= 9.93944 + 0.032695T – 0.017663pH + 0.001640C + 0.000027TC + 0.000424T^2 – 1.65373E-06C^2
	Rejection equation	= 101.05726 – 0.033963T – 0.034278pH – 0.000440C – 0.000028TC – 0.000288T^2 + 9.23922E-07C^2
Ion: Mg Membrane: MIL-101-Cr/IPN	Flux equation	= 9.58572 + 0.029364T – 0.016636pH + 0.001597C + 0.000027TC + 0.000424T^2 – 1.65373E-06C^2
	Rejection equation	= 101.17312 – 0.033963T – 0.034278pH – 0.000355C – 0.000028TC – 0.000288T^2
Ion: Na Membrane: GO/IPN	Flux equation	= 9.64071 + 0.013924T – 0.007237pH + 0.001568C + 0.000027TC + 0.000424T^2 – 1.65373E-06C^2
	Rejection equation	= 101.17984 – 0.038622T – 0.042764pH – 0.001024C – 0.000028TC – 0.000288T^2 + 9.23922E-07C^2
Ion: Mg Membrane: GO/IPN	Flux equation	= 9.21319 + 0.010593T – 0.006210pH + 0.001525C + 0.000027TC + 0.000424T^2 – 1.65373E-06C^2
	Rejection equation	= 101.28520 – 0.038622T – 0.042764pH – 0.000939C – 0.000028TC – 0.000288T^2 + 9.23922E-07C^2

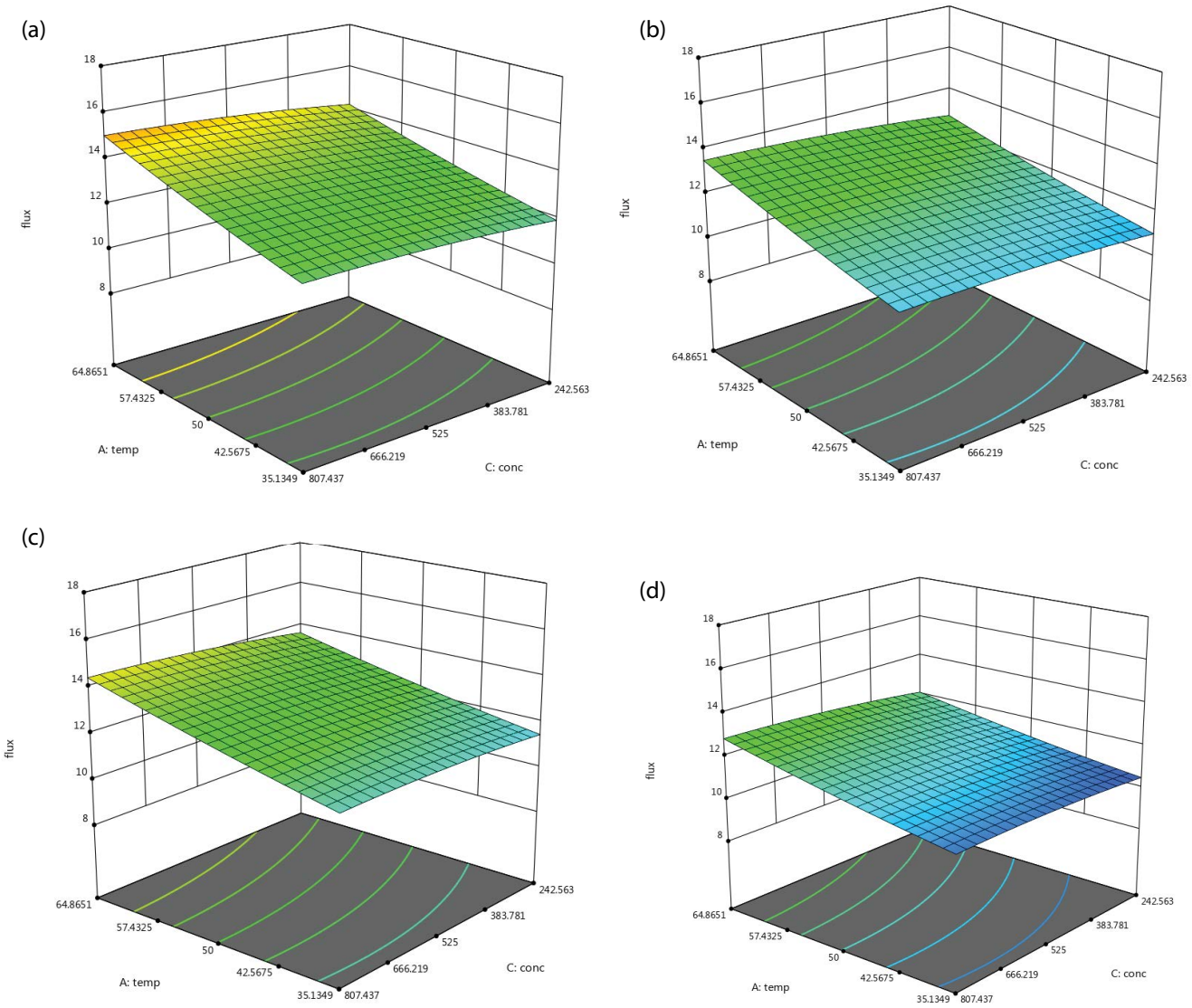

Fig. 10. 3D charts of flux vs. feed temperature vs. feed concentration, (a) MIL-101-Cr/IPN and Na ion, (b) GO/IPN and Na ion, (c) MIL-101-Cr/IPN and Mg ion, and (d) GO/IPN and Mg ion.

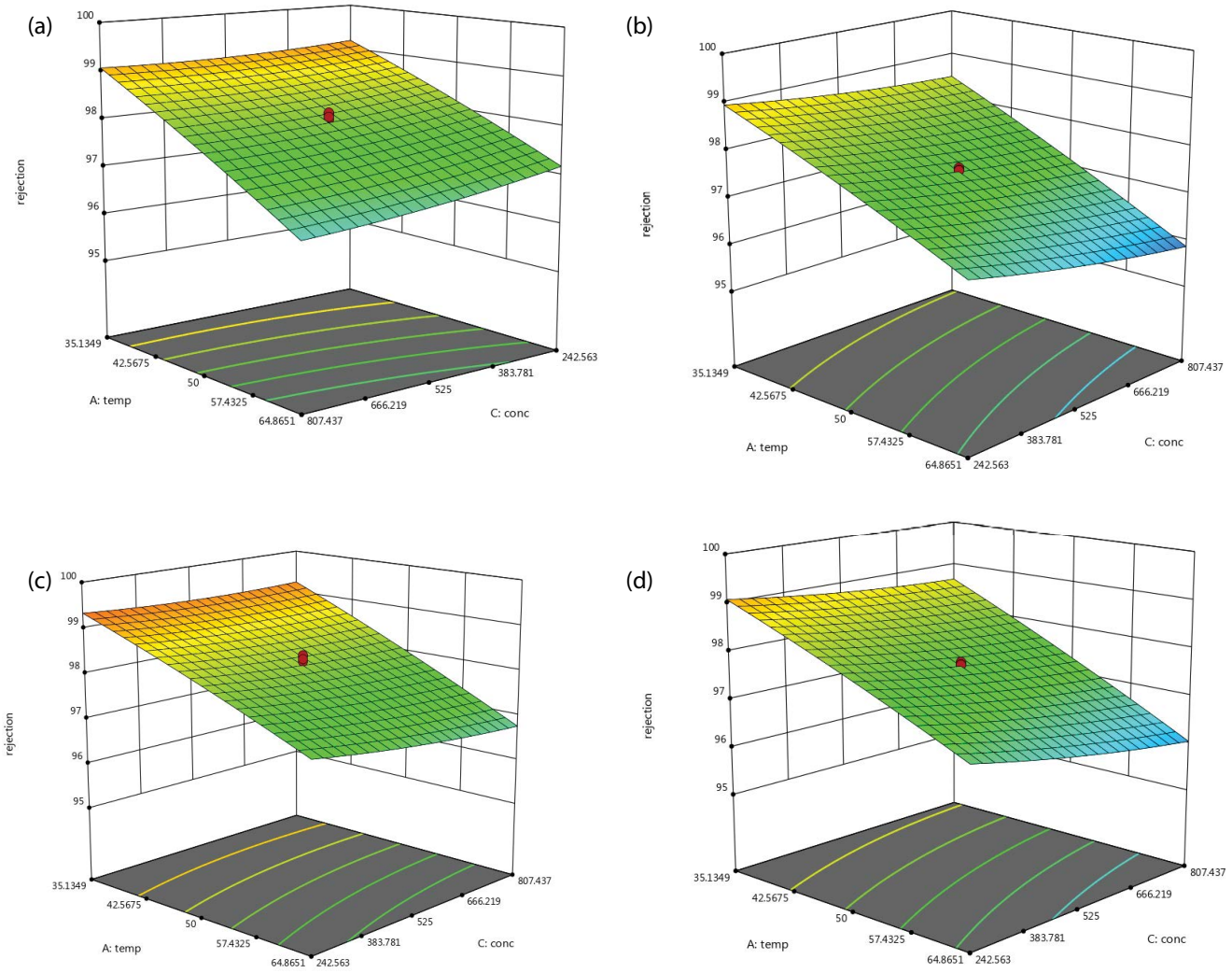

Fig. 11. 3D charts of salt rejection vs. feed temperature vs. feed concentration, (a) MIL-101-Cr/IPN and Na ion, (b) GO/IPN and Na ion, (c) MIL-101-Cr/IPN and Mg ion, and (d) GO/IPN and Mg ion.

may be due to the increase in the mobility of particles at high temperature and the decrease in the order of the polymer network of the membrane. However, the stability of the membrane decreased significantly by increasing the temperature of the feed solution.

Also, with an increase in the feed concentration, the flux decreased slightly, which may be caused by the fouling of the membrane pores by the salt particles. On the other hand, with an increase in feed temperature, the amount of salt rejection decreased significantly, which may be because the order of the membrane decreased at high temperature, and more salt particles were allowed to pass through the membrane.

With an increase in feed concentration, the amount of salt rejection decreased, which may be caused by the increase of particles in contact with the membrane surface, and the more this contact is, the greater the probability of particles penetrating into the membrane (Fig. 11).

For both ions, the amount of flux increased and repulsion decreased with the acidification of the feed. So, if the maximum amount of flux and repulsion is needed at the same time, it is better to operate at almost neutral pH.

Finally, according to CCD calculations, the MIL-101-Cr composite membrane showed more flux and salt rejection for both ions than the GO composite membrane. The maximum flux and salt rejection of MIL-101-Cr membrane for sodium ion were 15.19 kg/m^2·h and 99.24%, respectively. The highest flux and rejection of GO membrane for sodium ion were 13.65 kg/m^2·h and 98.97%, respectively. These values for magnesium ion were 14.59 kg/m^2·h and 99.37% by MIL-101-Cr membrane and 12.98 kg/m^2·h and 99.10% by GO membrane (Fig. 12).

3.9. Application of composite membrane in salt mixture

Various mixtures were made with different percentages of sodium and magnesium salts, and the flux and salt rejection were obtained under the optimum conditions using the MIL-101-Cr/IPN membrane (Table 2). Based on the data, as the percentage of magnesium increased in the mixture,

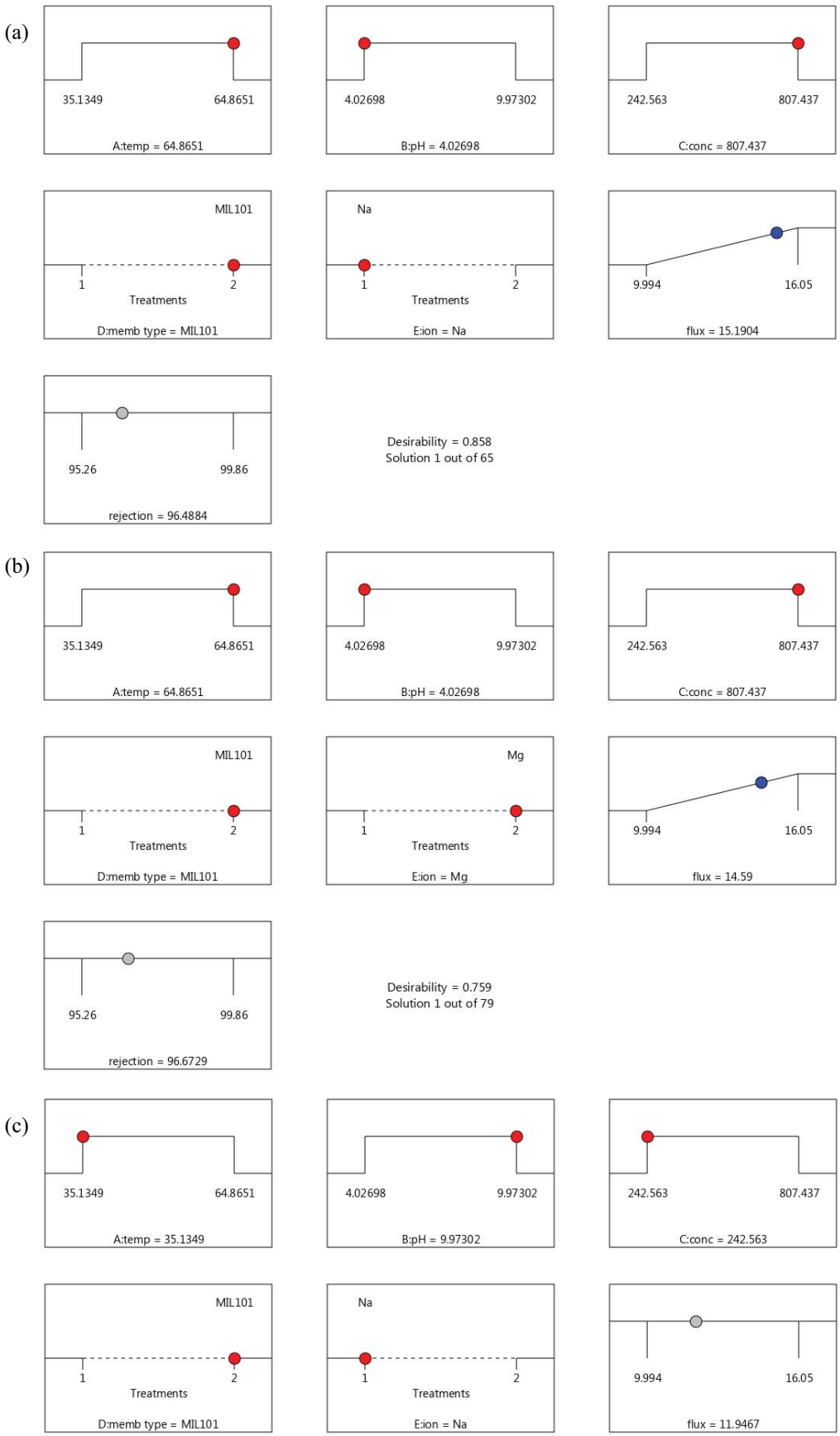

Fig. 12 (Continued)

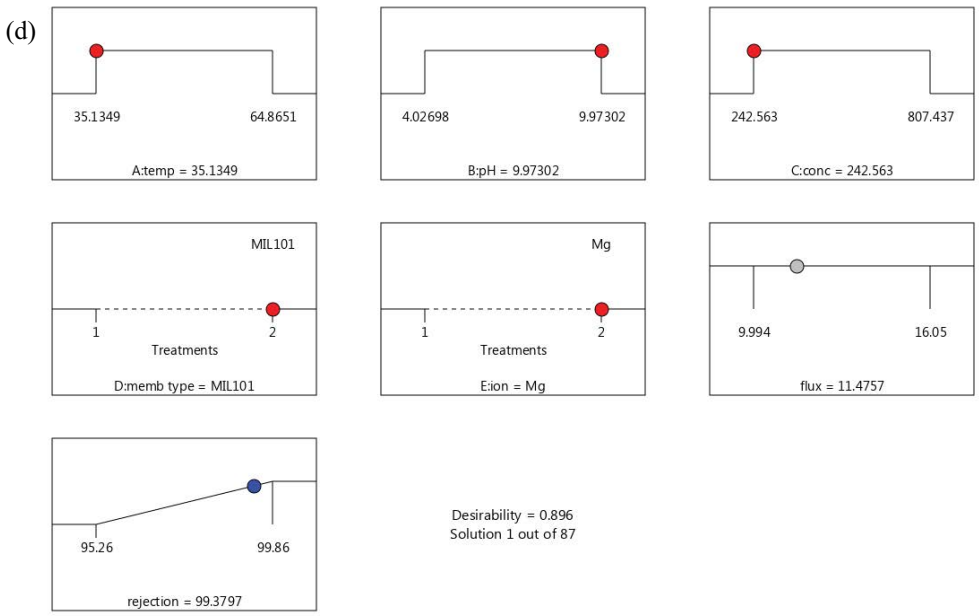

Fig. 12. Optimum conditions to obtain: (a) maximum flux of Na, (b) maximum flux of Mg, (c) maximum rejection of Na and (d) maximum rejection of Mg.

Table 2
Application of MIL-101-Cr/IPN membrane in salt mixture

Na (mg/L)	Mg (mg/L)	Na rejection	Mg rejection	Flux (kg/m²·h)
500	0	98.12	100	14.89
400	100	98.36	98.96	14.52
300	200	98.76	98.57	14.31
200	300	99.01	98.12	14.11
100	400	99.19	97.86	13.91
0	500	100	97.71	13.76

Table 3
Compare this work with other works

Membrane	Method	Flux (kg/m²·h)	Rejection%	References
Activated GO/PEI	Facile vacuum filtration	7	55	[48]
TA/GO/PEI	Vacuum assisted filtration	15.4	64	[49]
NH_2/MIL-53(Al)	MD	6.2	99.9	[50]
ZiF8/$(TA\text{-}Zn^{2+})_2$/PES	NF	5.1	93.6	[51]
ZiF8/TA/PES	NF	3.6	92.2	[36]
PVP/UiO-66-NH_2	NF	130	6.1	[35]
GO/COOH	–	4.9	40	[52]
MIL-101-Cr/IPN	Pervaporation	15.2	99.2	This work
GO/IPN	Pervaporation	13.6	98.9	This work

less flux was observed, which could be due to magnesium being bulkier compared to sodium, resulting in membrane fouling. Therefore, as the percentage of each type of salt increases in the mixture, the membrane rejection decreases compared to it.

3.10. Compare this work with other composite membrane works

Compared to other composite membranes used in previous works, the membrane used in this study showed very good performance in terms of both flux and salt rejection (Table 3).

4. Conclusion

Several composite membranes of IPN/MOF and IPN/GO were prepared using a sequential synthesis method, and their ability for desalination was examined. The two membranes that exhibited the best performance were selected. The IPN part of the membrane consisted of a hydrophilic polymer network of PVA and PAA, cross-linked by EGDMA and GA. The prepared membranes were evaluated and identified by swelling, contact angle, FTIR, tensile, and SEM tests. The membrane preparation was optimized using the experimental design method, and the optimal membranes were used for the desalination of NaCl and $MgCl_2$ salts using the pervaporation method. The IPN/MIL-101-Cr composite membrane showed better performance than GO, in terms of both flux and salt rejection. This could be due to the more hydrophilic properties and more specific action of MIL-101-Cr in absorbing water. This membrane had high mechanical stability, and it is hoped that it could be used in the industry for water purification by pervaporation, with modifications to other membrane methods.

References

[1] S.J. Lee, H.W. Lim, S.H. Park, Adsorptive seawater desalination using MOF-incorporated Cu-alginate/PVA beads: ion removal efficiency and durability, Chemosphere, 268 (2020) 128797, doi: 10.1016/j.chemosphere.2020.128797.

[2] M. Qasim, M. Badrelzaman, N.N. Darwish, N.A. Darwish, N. Hilal, Reverse osmosis desalination: a state-of-the-art review, Desalination, 459 (2019) 59–104.

[3] A. Liponi, C. Wieland, A. Baccioli, Multi-effect distillation plants for small scale seawater desalination: thermodynamic and economic improvement, Energy Convers. Manage., 205 (2020) 22–37.

[4] G.J. Doornbusch, M. Tedesco, J.W. Post, Z. Borneman, K. Nijmeijer, Experimental investigation of multistage electrodialysis for seawater desalination, Desalination, 464 (2019) 105–114.

[5] C. Xie, L. Zhang, Y. Liu, Q. Lv, G. Ruan, S.S. Hosseini, A direct contact type ice generator for seawater freezing desalination using LNG cold energy, Desalination, 435 (2018) 293–300.

[6] N. Ghaffour, S. Soukane, J.G. Lee, Y. Kim, A. Alpatova, Membrane distillation hybrids for water production and energy efficiency enhancement: a critical review, Appl. Energy, 254 (2019) 11–36.

[7] J.M. Gohil, A.K. Suresh, Chlorine attack on reverse osmosis membranes: mechanisms and mitigation strategies, J. Membr. Sci., 541 (2017) 108–126.

[8] C.Y. Tang, T.H. Chong, A.G. Fane, Colloidal interactions and fouling of NF and RO membranes: a review, Adv. Colloid Interface Sci., 164 (2011) 126–143.

[9] S. Amnuaypanicha, J. Patthana, P. Phinyocheep, Mixed matrix membranes prepared from natural rubber/poly(vinyl alcohol) semi-interpenetrating polymer network (NR/PVA semi-IPN) incorporating with zeolite 4A for the pervaporation dehydration of water–ethanol mixtures, Chem. Eng. Sci., 64 (2009) 4908–4918.

[10] M.N. Hyder, R.Y.M. Huang, P. Chen, Correlation of physicochemical characteristics with pervaporation performance of poly(vinyl alcohol) membranes, J. Membr. Sci., 283 (2006) 281–290.

[11] S.I. Semenova, H. Ohya, K. Soontarapa, Hydrophilic membranes for pervaporation: an analytical review, Desalination, 110 (1997) 251–286.

[12] S. Xiao, R.Y.M. Huang, X. Feng, Preparation and properties of trimesoyl chloride crosslinked poly(vinyl alcohol) membranes for pervaporation dehydration of isopropanol, J. Membr. Sci., 286 (2006) 245–254.

[13] S.G. Adoor, L.S. Manjeshwar, B. Vijay Kumar Naidu, M. Sairam, T.M. Aminabhavi, Poly(vinyl alcohol)/poly(methyl methacrylate) blend membranes for pervaporation separation of water+isopropanol and water+1,4-dioxane mixtures, J. Membr. Sci., 280 (2006) 594–602.

[14] Q. Zhao, J. Qian, Q. An, Z. Zhu, P. Zhang, Y. Bai, Studies on pervaporation characteristics of polyacrylonitrile–*b*-poly(ethylene glycol)–*b*-polyacrylonitrile block copolymer membrane for dehydration of aqueous acetone solutions, J. Membr. Sci., 311 (2008) 284–293.

[15] P. Shao, R.Y.M. Huang, X. Feng, W. Anderson, R. Pal, C.M. Burns, Composite membranes with an integrated skin layer: preparation, structural characteristics and pervaporation performance, J. Membr. Sci., 254 (2005) 1–11.

[16] M. Elma, C. Yacou, D.K. Wang, S. Smart, J.C. Diniz Da Costa, Microporous silica-based membranes for desalination, Water, 4 (2012) 629–649.

[17] C.H. Cho, K.Y. Oh, S.K. Kim, J.G. Yeo, P. Sharma, Pervaporative seawater desalination using NaA zeolite membrane: mechanisms of high-water flux and high salt rejection, J. Membr. Sci., 371 (2011) 226–238.

[18] S.G. Chaudhri, B.H. Rajai, P.S. Singh, Preparation of ultra-thin poly(vinyl alcohol) membranes supported on polysulfone hollow fiber and their application for production of pure water from seawater, Desalination, 367 (2015) 272–284.

[19] E. Huth, S. Muthu, L. Ruff, J.A. Brant, Feasibility assessment of pervaporation for desalinating high-salinity brines, J. Water Reuse Desal., 4 (2014) 109–124.

[20] B. Liang, K. Pan, L. Li, E. Giannis, B. Cao, High performance hydrophilic pervaporation composite membranes for water desalination, Desalination, 347 (2014) 199–206.

[21] M. Sule, J. Jiang, M. Templeton, E. Huth, J. Brant, T. Bond, Salt rejection and water flux through a tubular pervaporative polymer membrane designed for irrigation applications, Environ. Technol., 34 (2013) 1329–1339.

[22] M. Naim, M. Elewa, A. El-Shafei, A. Moneer, Desalination of simulated seawater by purge-air pervaporation using an innovative fabricated membrane, Water Sci. Technol., 72 (2015) 785–793.

[23] Q. Wang, Y. Lu, N. Li, Preparation, characterization and performance of sulfonated poly(styrene-ethylene/butylene-styrene) block copolymer membranes for water desalination by pervaporation, Desalination, 390 (2016) 33–46.

[24] D.A.R.O. da Silva, L.C.B. Zuge, A. de Paula Scheer, Preparation and characterization of a novel green silica/PVA membrane for water desalination by pervaporation, Sep. Purif. Technol., 247 (2020) 116852, doi: 10.1016/j.seppur.2020.116852.

[25] C. Zhao, Z. Jiang, J. Zhao, K. Cao, Q. Zhang, F. Pan, High pervaporation dehydration performance of the composite membrane with an ultrathin alginate/poly(acrylic acid)–Fe_3O_4 active layer, Ind. Eng. Chem. Res., 53 (2014) 1606–1616.

[26] A.P. Mathew, S. Packirisamy, H.J Radusch, S. Thomas, Effect of initiating system, blend ratio and crosslink density on the mechanical properties and failure topography of nano-structured full-interpenetrating polymer networks from natural rubber and polystyrene, Eur. Polym. J., 37 (2001) 1921–1934.

[27] L.H. Sperling, Interpenetrating Polymer Networks and Related Materials, Plenum, 1981.

[28] M. Kadhom, W. Hu, B. Deng, Thin film nanocomposite membrane filled with metal-organic frameworks UiO-66 and MIL-125 nanoparticles for water desalination, Membranes, 7 (2017) 31, doi: 10.3390/membranes7020031.

[29] T.C. Bowen, R.D. Noble, J.L. Falconer, Fundamentals and applications of pervaporation through zeolite membranes, J. Membr. Sci., 245 (2004) 1–33.

[30] A. Malekpour, M.R. Millani, M. Kheirkhah, Synthesis and characterization of a NaA zeolite membrane and its applications for desalination of radioactive solutions, Desalination, 225 (2008) 199–208.

[31] A. Malekpour, A. Samadi-Maybodi, M.R. Sadati, Desalination of aqueous solutions by LTA and MFI zeolite membranes using pervaporation method, Braz. J. Chem. Eng., 28 (2011) 669–677.

[32] B. Liang, W. Zhan, G. Qi, S. Lin, Q. Nan, Y. Liu, B. Cao, K. Pan, High performance graphene oxide/polyacrylonitrile composite pervaporation membranes for desalination applications, J. Mater. Chem. A, 3 (2015) 5140–5147.
[33] M. Jafarian, A. Malekpour, G.A. Koohmareh, Desalination of aqueous solutions using interpenetrating polymeric membranes-integrated zeolite through pervaporation and reverse osmosis, Desal. Water Treat., 286 (2023) 16–28.
[34] S. Bhattacharjee, C. Chen, W.-S. Ahn, Chromium terephthalate metal–organic framework MIL-101: synthesis, functionalization, and applications for adsorption and catalysis, RSC Adv., 4 (2014) 52500–52525.
[35] P. Zhao, R. Li, W. Wu, J. Wang, J. Liu, Y. Zhang, *In-situ* growth of polyvinylpyrrolidone modified Zr-MOFs thin-film nanocomposite (TFN) for efficient dyes removal, Composites, Part B, 176 (2019) 107208, doi: 10.1016/j.compositesb.2019.107208.
[36] Y. Xu, Y. Xiao, W. Zhang, H. Lin, L. Shen, R. Li, Y. Jiao, B.O. Liao, Plant polyphenol intermediated metal-organic framework (MOF) membranes for efficient desalination, J. Membr. Sci., 618 (2021) 118726, doi: 10.1016/j.memsci.2020.118726.
[37] A. Rajput, V. Yadav, P.P. Sharma, V. Kulshrestha, Synthesis of SGO composite interpenetrating network (CIPN) cation exchange membranes: stability and salt removal efficiency, J. Membr. Sci., 564 (2018) 44–52.
[38] M.M. Ghazi, A. Bagherian, The influence of anion-stripped MIL-101(Cr) dispersed in thin-film polyvinyl alcohol membrane matrix on the methylene blue dye separation, Coatings, 12 (2022) 1148, doi: 10.3390/coatings12081148.
[39] A.M.P. Peedikakkal, I.H. Aljundi, Mixed-metal Cu-BTC metal–organic frameworks as a strong adsorbent for molecular hydrogen at low temperatures, ACS Omega, 44 (2020) 28493–28499.
[40] D.T. Lee, J. Zhao, C.J. Oldham, G.W. Peterson, G.N. Parsons, UiO-66-NH_2 metal–organic framework (MOF) nucleation on TiO_2, ZnO, and Al_2O_3 atomic layer deposition-treated polymer fibers: role of metal oxide on MOF growth and catalytic hydrolysis of chemical warfare agent simulants, ACS Appl. Mater. Interfaces, 9 (2017) 44847–44855.
[41] D.R. Dreyer, S. Park, C.W. Bielawski, R.S. Ruoff, The chemistry of graphene oxide, Chem. Soc. Rev., 39 (2010) 228–240.
[42] G. Férey, C. Mellot-Draznieks, C. Serre, F. Millange, J. Dutour, S. Surblé, I. Margiolaki, A chromium terephthalate-based solid with unusually large pore volumes and surface area, Science, 309 (2005) 2040–2042, doi: 10.1126/science.1116275.
[43] A.M.P. Peedikakkal, A.A. Jimoh, M.N. Shaikh, B.E. Ali, Mixed-metal metal–organic frameworks as catalysts for liquid-phase oxidation of toluene and cycloalkanes, Arabian J. Sci. Eng., 42 (2017) 4383–4390.
[44] S. Farhadi, F. Mahmoudi, M.M. Amini, M. Dusek, M. Jarosova, Synthesis and characterization of a series of novel perovskite-type $LaMnO_3$/Keggin-type polyoxometalate hybrid nanomaterials for fast and selective removal of cationic dyes from aqueous solutions, Dalton Trans., 10 (2017) 3252–3264.
[45] T.-T. Zhu, Z.-M. Zhang, W.-L. Chen, Z.-J. Liu, E.-B. Wang, Encapsulation of tungstophosphoric acid into harmless MIL-101(Fe) for effectively removing cationic dye from aqueous solution, RSC Adv., 6 (2016) 81622–81630.
[46] S. Gahlot, P.P. Sharma, V. Kulshrestha, P.K. Jha, SGO/SPES-based highly conducting polymer electrolyte membranes for fuel cell application, ACS Appl. Mater. Interfaces, 6 (2014) 5595–5601.
[47] T. Wang, Y. Li, S. Geng, C. Zhou, X. Jia, F. Yang, L. Zhang, X. Ren, H. Yang, Preparation of flexible reduced graphene oxide/poly(vinyl alcohol) film with superior microwave absorption properties, RSC Adv., 5 (2015) 88958–88964.
[48] P.S. Parsamehr, M. Zahed, M. Ahmadzadeh, T. Mohammadi, M. Rezakazemi, Preparation of novel cross-linked graphene oxide membrane for desalination applications using (EDC and NHS)-activated graphene oxide and PEI, Desalination, 468 (2019) 114079, doi: 10.1016/j.desal.2019.114079.
[49] M.Y. Lim, Y.S. Choi, J. Kim, K. Kim, H.S. Shin, J.J. Kim, D.M. Shin, J.C. Lee, Cross-linked graphene oxide membrane having high ion selectivity and antibacterial activity prepared using tannic acid-functionalized graphene oxide and polyethyleneimine, J. Membr. Sci., 521 (2017) 1–9.
[50] J. Zuo, T.-S. Chung, Metal-organic framework-functionalized alumina membranes for vacuum membrane distillation, Water, 586 (2016) 1–15.
[51] Y. Xiao, W. Zhang, Y. Jiao, Y. Xu, H. Lin, Metal-phenolic network as precursor for fabrication of metal-organic framework (MOF) nanofiltration membrane for efficient desalination, J. Membr. Sci., 624 (2021) 119101, doi: 10.1016/j.memsci.2021.119101.
[52] Y. Yuan, X. Gao, Y. Wei, X. Wang, J. Wang, Y. Zhang, C. Gao, Enhanced desalination performance of carboxyl functionalized graphene oxide nanofiltration membranes, Desalination, 405 (2017) 29–39.